Nanotechnology Perceptions
ISSN 1660-6795
www.nano-ntp.com

Passive 6G MIMO Antenna Design for High Gain Using CST Simulation Software

Narayan Krishan Vyas, Dr. R. P. Yadav, Mohhamad Salim

Department of Electronics Communication Engineering, Malaviya National Institute of Technology Jaipur, Rajasthan, India

Mobile communication networks have improved speech and data capabilities from the First Generation (1G) to the Fifth Generation (5G), overcoming the constraints of their predecessors. The development of sixth-generation (6G) technology would improve data throughput, latency, connectivity, dependability, and energy efficiency. Due to its tiny size, flexibility, and cost-effectiveness, microstrip patch antennas are attractive technologies for high-gain passive 6G Multiple-Input Multiple-Output (MIMO) antennas. The proposed methodology entails integrating Internet of Things (IoT) devices with the 5G channel, optimizing data transmission, and evaluating the potential of the 6G channel for managing a variety of data-intensive applications. This research seeks to contribute to the creation of passive 6G MIMO antennas with high gain for revolutionary wireless communication applications. The patch antenna model was subjected to extensive analysis, which included S-parameter evaluation (2.06 - 4.68 GHz), balance measurements (2.00 - 9.09 GHz), Y/Z-matrix elements, field energy, Voltage Standing Wave Ratio (VSWR), and directivity plots. 3D findings showed a passive 6G MIMO antenna with high gain. Analysis of electric and magnetic field distributions, directivity plots, axial ratio, and polarization phase revealed its performance and polarization properties.
Keywords: Network, Communication, MIMO, Antenna, Microstrip Patch Antenna, Frequency.

1. Introduction

The initial objective of the mobile communication networks of the First Generation (1G) that launched in the 1980s was to facilitate voice communication through analog mobile technology [1]. Second-generation (2G) mobile communication technologies introduced a digital network to overcome the shortcomings of its analog predecessors. The 1990s saw the

beginning of widespread support for data applications like SMS, or short messaging service. Third-generation (3G) mobile broadband services made possible the development of innovative new applications including multimedia messaging services, video calls, and mobile television. The advent of 4G technology allowed for the development of more advanced mobile internet services, the streaming of high-definition videos, and the practice of seamless handover. Quality of Service (QoS) levels were created with the widespread deployment of IP-based communication to accommodate a wide range of customer needs [2]. As a consequence of that, there has been a meteoric rise in the quantity of wirelessly linked gadgets as technology progressed [3]. Antennas have become a significant technology and the most discussed subject in the field of wireless communication in recent decades, making the development of broadband and high-gain antennas that span a wide frequency range imperative [4].

The development of 5G mobile communication networks has been a game-changer. Data rates (10 Gbps), latency (1 millisecond), connectivity (1 million/km2), dependability (105), and energy usage are only some of the standards that the network must meet to enable 5G [5]. Expectations for the Sixth Generation (6G) remain unclear due to the lack of detail regarding its predicted architecture and performance components. MIMO technologies, such as massive MIMO (mMIMO) [6], exceptionally large MIMO (XL-MIMO) [7], Intelligent Reflecting Surfaces (IRS) [8-9], and Cell-Free mMIMO (CF-mMIMO) [10], are among the most promising developments in the field of 6G Networks. Antennas with MIMO are well suited for high-speed, high-quality mobile communication systems like 5G and 6G [11]. From an implementation standpoint, it is tricky to accommodate several components on a portable terminal, and it is also difficult to create space between the terminals [12-13]. As can be seen in Figure 1, a ground plane is located below the dielectric material.

Figure 1. Microstrip patch antenna [14].

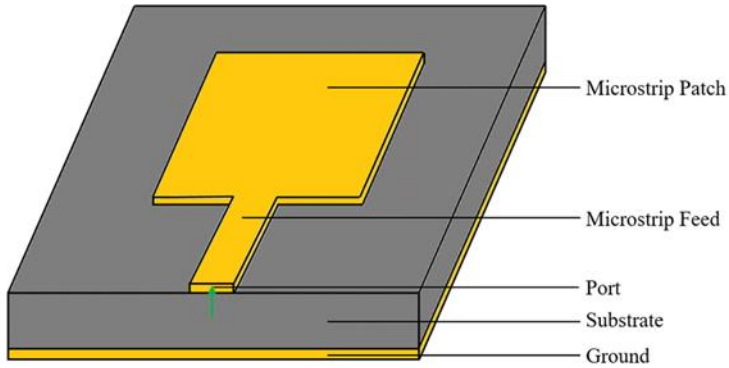

The terminals of microstrip patch antennas are typically tiny, lightweight, flexible, and inexpensive, and the antennas themselves are simple to fabricate using a standard microstrip manufacturing method [15-16]. These benefits of microstrip patch antennas have led to their widespread usage in a wide variety of fields, including telemetry and communication, GPS systems, naval communications, and Radio Frequency Identification (RFID) [17-18]. The research's goals are to specify the antenna's shape and arrangement, settle on a frequency band suitable for 6G networks, and fine-tune the layout for maximum gain. The suggested antennas'

material selection, mutual coupling mitigation, and resilience under varying environmental circumstances could be explored with the use of precise and verified electromagnetic models created using Computer Simulation Technology (CST) simulation software. The study's overarching goal is to aid in the development of high-gain passive 6G MIMO antennas that are efficient and reliable for use in revolutionary 6G wireless communication applications by identifying design trade-offs and optimizing antenna parameters to achieve the best compromise between conflicting goals. Antenna engineers have a great tool in CST simulation software for modeling, simulating, and optimizing complicated antenna systems in the 6G frequency band. Its capacity to do numerical simulations makes it possible to assess the performance of a variety of antenna designs accurately and reliably, materials, and feeding methods. The study follows the following structure: In Section 2, the authors provide a literature review on passive 6G MIMO antenna design for high gain using CST simulation software. The study methodology and methods are introduced in Section 3, and the recommended method is proven. The latter section is the basis for the anticipated findings presented in Section 4. The report then comes to a conclusive verdict and provides suggestions for areas that need more research in section 5.

Overview of 6G Technologies

Each successive generation, ranging from 1G to 5G, has introduced numerous advancements. Despite being at the current stage of implementation, the 5G mobile communication technology exhibits various difficulties encompassing elevated data traffic, latency, security concerns, energy efficiency, and frequency band allocation [19-20]. Given these shortcomings of 5G, development has already begun on 6G systems, which would include several novelties and technology that its predecessors lacked. Machine-type communication would advance when networks are forced to exchange larger volumes of data at fast speeds, linking not just people but also machines, gadgets, and sensors. Without a doubt, the idea of ubiquitous Artificial Intelligence (AI) has made 6G a popular issue in the scientific community. The key driver behind the adoption of 6G would be the growth of AI's tremendous usefulness [21]. The authors anticipate that 6G would improve upon 5G in several ways.

Figure 2 highlights six key factors, namely frequency, peak data rate, individual data rate, mobility, spectrum efficiency, and delay [22]. A better spectrum efficiency, lower latency, higher frequency and data transmission rate, greater mobility, and faster reaction times are all required for 6G, as shown in Figure 2. Table 1 provides information on the 6G KPIs in a tabular format.

Figure 2 The vision of 6G [23].

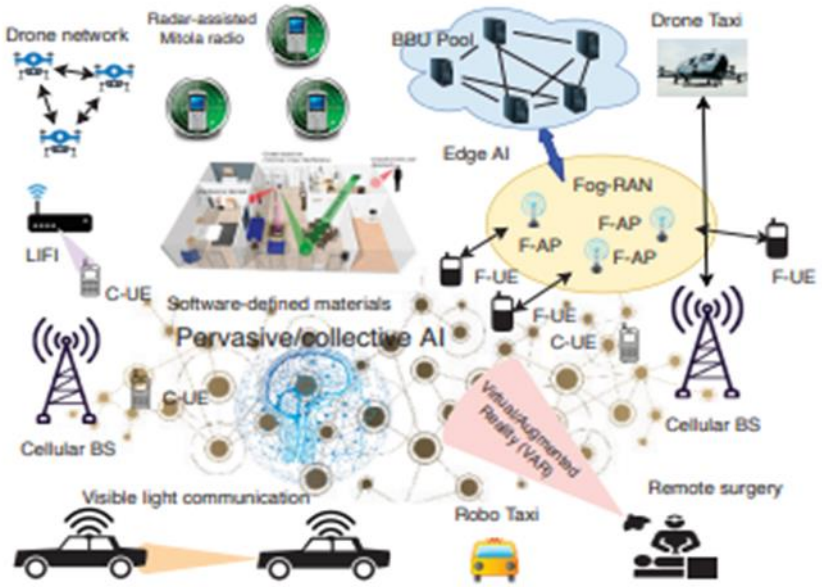

Table 1. 6G Necessities and Capabilities [24-26]

Requirements	6G
Service types	MBRLLC/m URLLC/HCS/MPS
Service level	Tactile
Device types	Smart implants/ CRAS/XR and BCI equipment/ Sensors and DLT devices
Jitters	1μsec
Individual data rate/Peak DL data rate	100 Gbps/≥1 Tbps
Latency/Mobility/Reliability	0.1 msec/ up to 1000km/h/ up to 99.99999%
Frequency bands/Multiplexing	Sub-THz band/Smart OFDMA plus IM

MIMO Antenna Design

MIMO antennas have garnered a lot of attention in current wireless communication systems because they can use multiple pathways to send or receive data, increasing range and output performance [27]. It is imperative to acknowledge that for distinct components of the MIMO antenna to effectively transmit or receive signals concurrently without compromising the antenna's properties, a significant level of isolation between the various elements within the same MIMO system is essential. It is not only the S-parameters and radiation characteristics of a MIMO antenna that are utilized to guarantee its quality; diversities parameters are also used. For MIMO antennas to be useful, they must conform to a set of predetermined values for diversity parameters. Because of this, this section discusses some of the most fundamental diversity parameters for MIMO antennas (Figure 3).

Figure 3 Parameter of MIMO Antenna

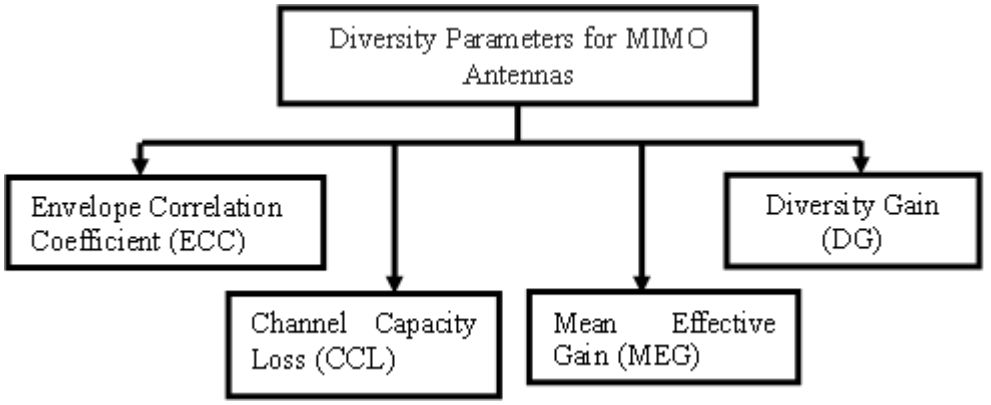

- Envelope Correlation Coefficient (ECC)

The ECC is used to determine the level of correlation between the antenna's elements. To increase the variety among the MIMO antenna components, it is necessary to allow for law correlations between the antenna elements [28]. Equation 1 provides the arithmetic equation for ECC based on the radiation pattern data from a MIMO architecture [29]:

$$\mathrm{ECC_{qp}} = \frac{\left|\int_0^{2\pi}\int_0^{\pi}\left(\mathrm{E_{\theta p}^{*}E_{\theta q}XPR+E_{\varphi p}^{*}E_{\varphi q}P_{\varphi}}\right)\mathrm{d\Omega}\right|^2}{\alpha\times\beta} \quad (1)$$

here,

$$\alpha = \int_0^{2\pi}\int_0^{\pi}\left(\mathrm{E_{\theta p}^{*}E_{\theta q}P_{\theta}XPR + E_{\varphi p}^{*}E_{\varphi q}P_{\varphi}}\right)\mathrm{d\Omega} \quad (2)$$

$$\beta = \int_0^{2\pi}\int_0^{\pi}\left(\mathrm{E_{\theta p}^{*}E_{\theta q}P_{\theta}XPR + E_{\varphi p}^{*}E_{\varphi q}P_{\varphi}}\right)\mathrm{d\Omega} \quad (3)$$

where XPR is the average power ratio between the phi and theta axes, indicating the degree of cross-polarization. The minimum allowable ECC in a real-world setting is 0.5.

- Diversity Gain (DG)

The diversity gain of a MIMO antenna is used to evaluate its performance and reliability in wireless networks. Therefore, within the permitted frequency range, the multiplexed antenna must have a high DG of 10 dB. The DG (2) can be determined by plugging in the value of the ECC into Equation 4 [30-31]:

$$\mathrm{DG} = 10 \times \sqrt{1 - \left|\mathrm{ECC_{qp}}\right|^2} \quad (4)$$

- Channel Capacity Loss (CCL)

The CCL is the maximum data rate that may be transmitted over a given communication channel with only a small amount of data being lost. The CCL is always 0.4 bits per second per hertz for every given MIMO system [32].

- Mean Effective Gain (MEG)

The MEG, or the ratio of MIMO antenna power to isotropic antenna power, is one of the most crucial diversity metrics for MIMO antennas. The ratio $\frac{\mathrm{MEG_i}}{\mathrm{MEG_j}}$ of a MIMO antenna with equal power output must be less than 3 dB for optimum performance. Equations 5 and 6 may be used to calculate the MEG [33]:

$$\mathrm{MEG_i} = 0.5\left[1 - |\mathrm{S_{ii}}|^2 - \left|\mathrm{S_{ij}}\right|^2\right] \quad (5)$$

And

$$\mathrm{MEG_j} = 0.5\left[1 - \left|\mathrm{S_{ij}}\right|^2 - \left|\mathrm{S_{jj}}\right|^2\right] \quad (6)$$

2. Literature of Review

This portion of the study is where the author defines the Literature review on the passive 6G MIMO antenna design for high gain utilizing CST simulation software.

Omrani et al., (2023) [34] developed an ultra-wideband Microstrip MIMO antenna designed to cover the frequency range of 2.4 to 6.5 GHz, which includes the Wireless Local Area Network (WLAN) and Sub-6G frequencies. The applicable MIMO antenna is made up of two microstrip antenna components that are mirror images of one another. Each microstrip is 0.250 of the lower band (2.5 GHz) in frequency and is built using the stepped impedance resonator (SIR) method. ECC values below 0.02 are seen over the whole frequency range. The results of the simulations show that the proposed microstrip MIMO antenna system using the multi-tiered EBG structure is ideal for WLAN and Sub-6G applications.

Musaed et al., (2022) [35] presented the tunability performance, idea, and evaluation of an innovative and Miniaturized Metamaterial (MTM) unit cell encompassing forthcoming 6G applications. Two Split-Ring Resonators (SRR) in the form of a star are the building blocks of the suggested metamaterial. The proposed MTM's comparable circuit is generated using numerical simulation in CST microwave studio and compared with that generated by Advanced Design Software (ADS), with both showing a similar transmission coefficient (S21).

Cui et al., (2022) [36] utilized the low-power capabilities of a 6G network to develop a communication system that incorporates Reconfigurable Intelligent Surface (RIS) and Artificial Intelligence (AI) technologies. It replaces the conventional phased array at the base station with an RIS consisting of 256 individual elements for improved hardware architecture. To further facilitate communication with significantly less transmission power, a 2304-element RIS is designed and deployed as a relay. To reduce the load on the server, they create an AI-based transmission layout for use in the program. Collaboratively developed hardware and software allow for the prototype to transmit 4K video in real-time with low power consumption.

Alsudani et al., (2022) [37] developed a finite-internal-model analysis of a rectangular Microstrip antenna (MPA) using the CST antenna simulation program for use in 28 GHz 5G

applications. Frequency-selective surfaces (FSSs) are incorporated to enhance the performance of the proposed MPA. The proposed MPA is situated amid two FSS superstrates; the upper superstratum functions as a passive bandpass filter, while the bottom superstratum reflects leaking radiation from the MPA's ground plane.

Shlezingerr et al., (2021) [38] offered a different use of Meta surfaces in wireless communications; specifically, as active reconfigurable antennas with high-end analog signal processing capabilities for transceivers of the future. It examines the benefits and drawbacks of using metasurfaces for radiation and reception and discusses how they could affect the reliability of communication in wireless networks. They describe several interesting research and implementation issues that come from the use of meta-surface antennas in wireless transceivers, noting that present studies only reveal a fraction of the potential of meta-surfaces.

Dai et al., (2020) [39] created a 256-element RIS with good gain at a minimal cost. The proposed RIS incorporates 2-bit phase shifting for beamforming using Positive Intrinsic-Negative (PIN) diodes, bringing together the operations of phase shifting and radiation on a single electromagnetic surface. The results show that using RISs in wireless communications is both practical and effective. The authors demonstrate a 21.7dBi antenna gain at 2.3 GHz with the suggested RIS. The antenna achieves a gain of 19.1 dBi at the mm-wave frequency of 28.5 GHz.

3. Technique Used

A mathematical method called the Lagrange Multiplier Method is utilized to resolve restricted optimization issues. When attempting to determine the maximum or lowest value of a function subject to one or more restrictions, it is very helpful. It could be thought of as the pace at which the objective function changes about how the inequality and equality constraint functions change [40]. If $[0\ 1] \times [0\ 1]$ is a compact set and $f(v, i)$ and $g(v, i)$ have continuous first partial derivatives, then the solution occurs. If $(v_s, i_s) \in \Omega_s \in \mathbb{R}^2$ and $f(v, i)$ is locally maximum in $(v_s, i_s) \in \Omega_s$, then the core formula of Lagrange multiplier techniques could be written as follows, where the scalar $\lambda \neq 0$ is the Lagrange multiplier:

$$\nabla f(v, i) - \lambda \nabla g(v, i) = 0^2 \qquad (7)$$

Where $\nabla f(v, i) = \left(\frac{\partial f(v,i)}{\partial v}, \frac{\partial f(v,i)}{\partial i}\right)$ and $\nabla g(v, i) = \left(\frac{\partial g(v,i)}{\partial v}, \frac{\partial g(v,i)}{\partial i}\right)$ are the gradient of the cost and constraint function $f(v, i)$ and $g(v, i)$ respectively. The gradient of $f(v, i)$ and $h_j(v, i)$ are given by [41]:

$$\nabla f(v, i) = V_{oc} I_{sc} \binom{i}{v}, \nabla h_1(v, i) = \binom{-1}{0}, \nabla h_2(v, i) = \binom{1}{0}, \nabla h_3(v, i) = \binom{0}{-1}, \nabla h_4(v, i) = \binom{0}{1}$$

4. Proposed Methodology

In this part, the author explains the suggested methodology, which is based on the passive design of the 6G MIMO antenna for high gain. Figure 4 illustrates the block diagram of the proposed work.

Figure 4 Block diagram of proposed work

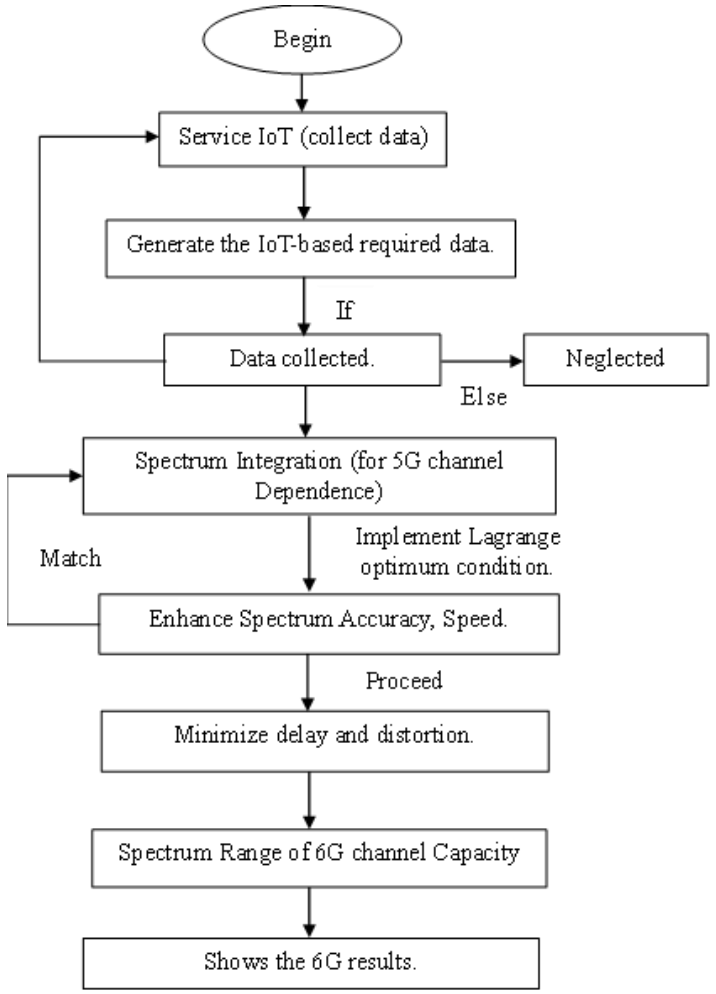

It starts the process and progresses to the next step, which is to set up the IoT service, which entails installing devices or sensors to gather data. To obtain meaningful information, such devices can be deployed over many places and linked to the network. When IoT devices are installed and functioning, they begin to generate data. Depending on the application, this data might include sensor readings, bandwidth, environmental data, or any additional relevant data. Following that, there looks to be a conditional statement stating that if data from IoT devices is successfully obtained, it would move to the following stages. If data collection fails for whatever reason, the operation may be stopped or postponed until the problem is rectified.

The data obtained from the IoT devices is then integrated with the 5G channel. Spectrum integration is the technique of transmitting data via 5G networks by leveraging several frequency bands within the electromagnetic spectrum. The next stage is to improve the accuracy and speed of data transmission across the 5G spectrum using the Lagrange optimization condition. The goal is most likely to increase the system's overall efficiency and

performance. Following that, it continues the optimization process by concentrating on decreasing data transmission delays and distortion. Low latency and low distortion are critical for real-time applications for delivering high-quality data. Finally, the paragraph ends with the phrase "6G channel capacity." This seems to be analyzing the potential of the 6G channel, most likely based on optimum spectrum usage and data from IoT devices. The findings of this research would aid in determining the 6G network's capability and potential for handling different data-intensive applications.

5. Simulation and Modeling

The microstrip patch antenna is a popular and versatile antenna type that is suitable for a wide variety of applications. Using numerous mathematical parameters, the efficacy of the patch antenna's initial model has been evaluated. Figure 5 depicts the initial model of a patch antenna consisting of a ground layer, substrate, patch, port 1, and port 2.

- Ground layer: The ground layer is an antenna's lower metal layer. It is employed to reflect electromagnetic radiation to the patch, thereby enhancing the antenna's directivity.
- Substrate: In between the ground plane and the patch is a dielectric substance known as the substrate. Both the patch's structural integrity and the antenna's electrical characteristics can be adjusted with its help.
- Patch: The patch is a metal layer placed on top of the substrate. It is the radiating element of the antenna and is responsible for producing electromagnetic radiation.
- Port 1: The antenna's input port is located at port 1. It serves to link the antenna to the signal source.
- Port 2: Port 2 serves as the load port for the antenna. The purpose of this component is to establish a connection between the antenna and the load.

Antenna performance is simulated using the initial patch antenna model.

Figure 5 Initial model.

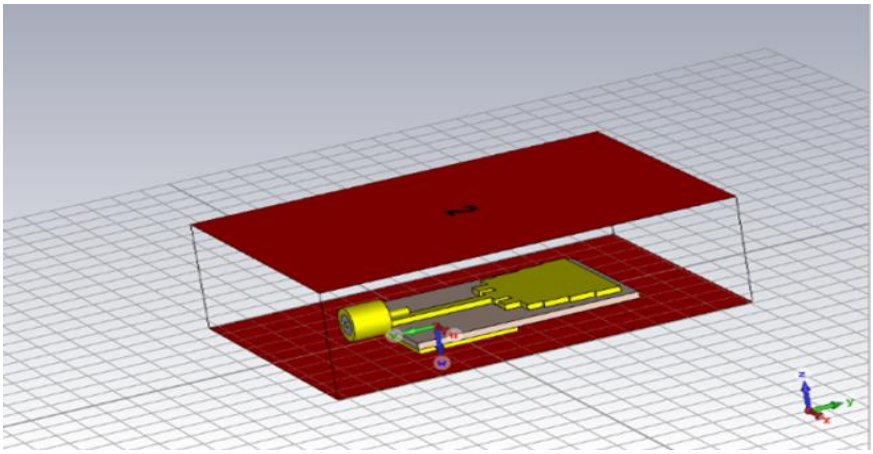

1-D Results

S-parameters for a two-port network are shown in Figure 6 at a variety of frequencies. The frequencies are between 2.06377 and 4.68257 gigahertz (GHz). S 1,1, S 1,2, S 2,1, and S 2,2 denote the S-parameters. S 1,1 and S 2,2 are parameters of reflection, whereas S 2,1 and S 1,2 are transmission parameters. These parameters characterize how a network responds to signals at various frequencies. At 2.06377 GHz, for instance, S 1,1 is about -5.52, S 2,1 is about -20.61, S 1,2 is about -23.33, and S 2,2 is about -6.93.

Figure 1 S-parameters at various frequencies for a two-port network

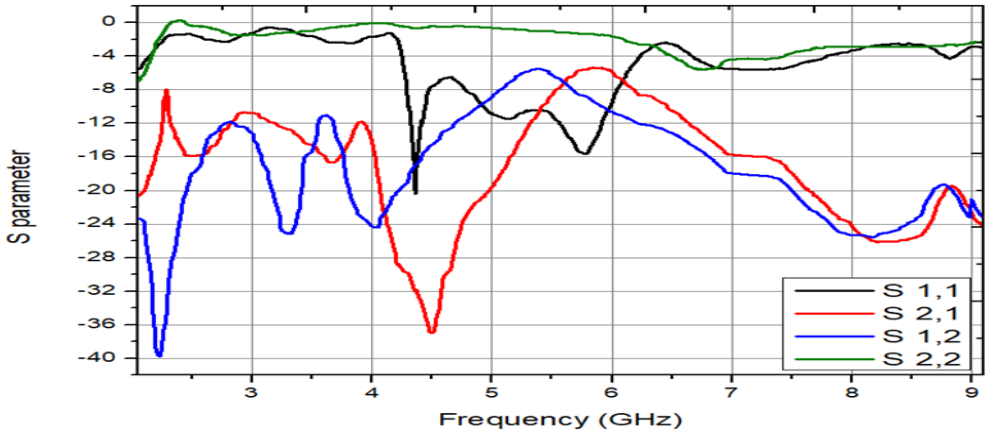

Figure 7 displays the results of a series of frequency-dependent balance measurements of the S-parameters, with two groups of values for the balance shown as "Balance [1]" and "Balance [2]." These readings were taken between 2.00766 GHz and 9.08892 GHz. Balance [1] varies between 0.2220787 and 0.950377, whereas Balance [2] ranges between 0.0220595 and 1.01634.

Figure 2 S-parameter balance

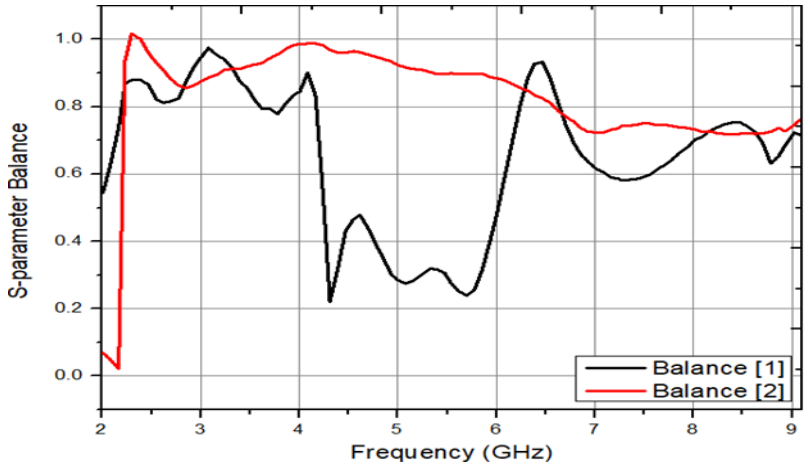

The Y-matrix is shown in Figure 8 at various frequencies (in GHz). In electrical engineering, the Y-matrix is a common mathematical representation used to characterize the performance

of linear electrical networks. Each of the four elements in this illustration represents a different set of input values and is labeled accordingly: Y_1,1, Y_2,1, Y_1,2, and Y_2,2. Figure 8 illustrates the frequency-dependent shifts in these parameters.

Figure 3 Y-matrix at different frequencies

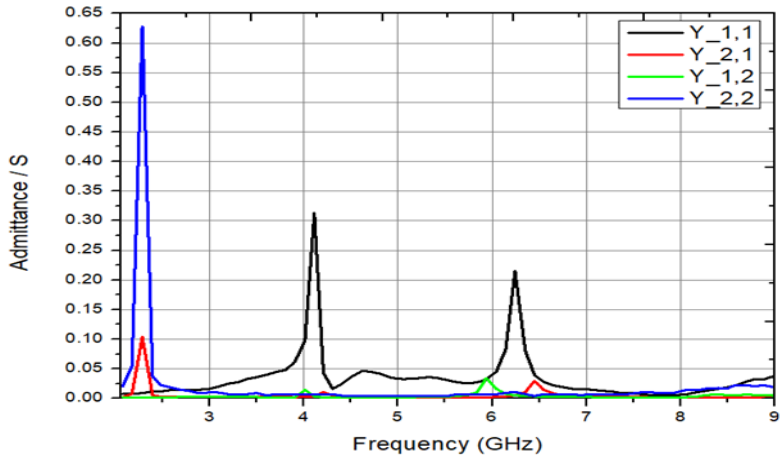

FIGURE 9: Impedance (in ohms) vs frequency (in GHz) for various elements specified by Z-matrix entries. The x-axis frequency ranges from 2 GHz to 9.10532 GHz, and the corresponding impedance values for Z_1,1, Z_2,1, Z_1,2, and Z_2,2 are provided. Across the frequency spectrum, the impedance values vary, reflecting the electrical behavior of the system. The graph provides an exhaustive view of how impedance varies with frequency, which is necessary for comprehending and analyzing the electrical properties of the Z-matrix elements.

Figure 4 Frequency vs. Impedance Matrix: Exploring Z-values at Different GHz

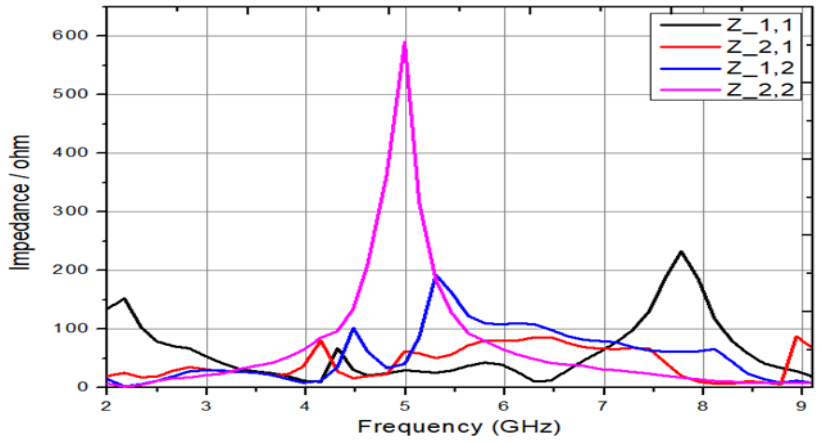

Figure 10 shows the energy in the field at discrete times (in nanoseconds) for two distinct energies (Energy [1] and Energy [2]). Energy quantities are tracked throughout time to demonstrate dynamics within a given system or procedure. The maximum field energy value in "Energy [1]" is -0.620389 at a frequency of 0.492464, while the minimum value is -113.992

at a frequency of 0.0283665. The maximum value for "Energy [2]" is -0.362845 at frequency 0.608488, while the minimum value is -39.1365 at frequencies 5.29165 and 5.39713.

Figure 5 Field Energy

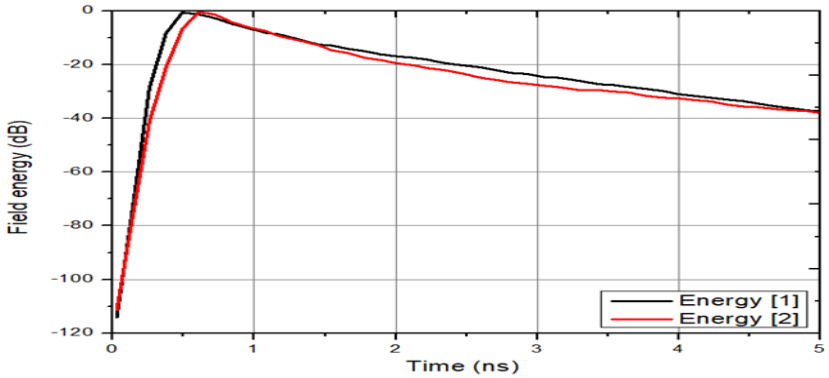

The graph in Figure 11 depicts the Voltage Standing Wave Ratio (VSWR) versus frequency in gigahertz (GHz). The VSWR values are displayed on the y-axis, while the corresponding frequencies are shown along the x-axis. The VSWR_1 and VSWR_2 are distinct collections of VSWR measurements. Both sets of VSWR values fluctuate as the frequency increases from approximately 2 GHz to nearly 9 GHz. Initially, at lower frequencies, VSWR values are comparatively high, indicating that impedance matching is inadequate. However, as frequency increases, VSWR values tend to decrease, indicating that impedance matching has been improved. This information provides insight into the efficacy of the investigated system or device across a spectrum of frequencies.

Figure 6 Voltage Standing Wave Ratio

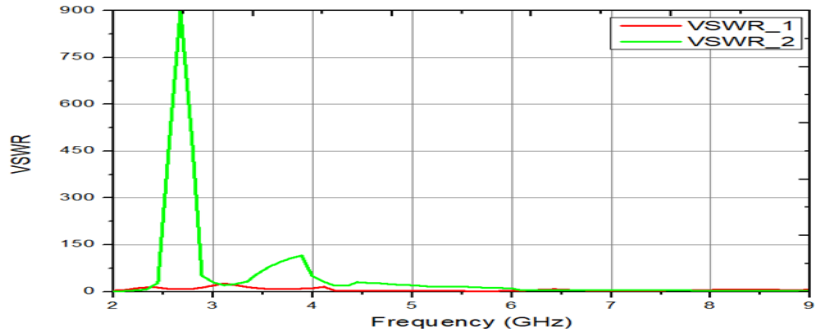

3-D Results

Figure 12 depicts the simulation result of a passive 6G MIMO antenna with a high gain designed using CST software. The antenna is composed of Rogers RO4350B material, operates at 6 GHz, and has two ports on opposite extremities. A maximum electric field strength of 450 V/m is observed at the extremities and a minimum at the center. This design strives for a 10 dBi gain, indicating its ability to efficiently direct electromagnetic energy. The lack of power input and the absence of transistors and amplifiers characterize it as passive. In order to achieve greater data speeds and more reliable communication, 6G MIMO systems,

which rely on numerous antennas for simultaneous data transmission and reception, could benefit from this antenna. Shown in Figure 12 (a) and (b) is the electric field at ports 1 and 2.

Figure 7 Electric Field at Port 1 and Port 2.

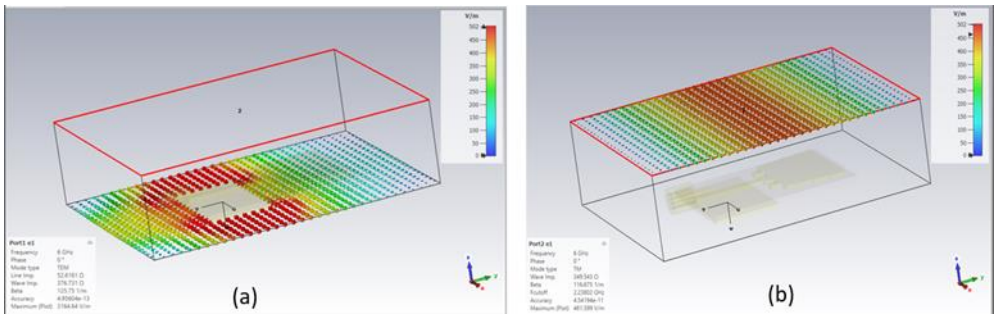

Figures 13 (a) and (b) show the magnetic field distribution at two different ports, namely Port 1 and Port 2, in the context of the passive 6G MIMO antenna design utilizing CST simulation software to achieve high gain. This illustration is helpful because it shows how the electromagnetic fields are spread and interact at various places, which affects the antenna system's overall performance and usefulness.

Figure 8 Magnetic Field at Port 1 and Port 2

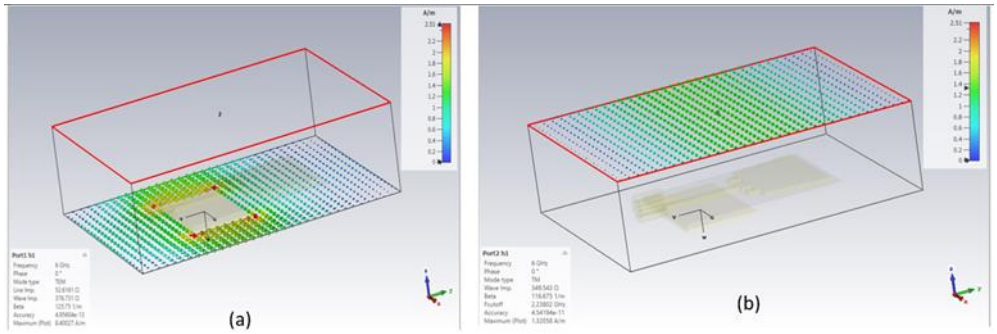

The existence of Ports 1 and 2 generates an electric field inside the antenna substrate, as shown in Figures 14 (a) and (b). These diagrams show, with great clarity, how the electric field is dispersed and modified at the various terminals.

Figure 9 Substrate electric field

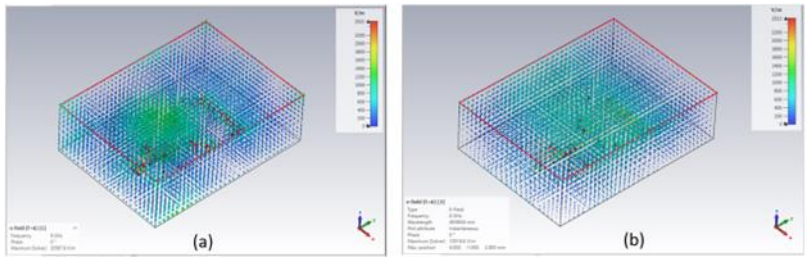

Magnetic field distributions within the substrate due to Port 1 and Port 2 are shown in Figure 15 (a) and (b). This illustration shows how the magnetic field within the substrate is affected

and interacted with by the presence of these two ports.

Figure 10 Substrate Magnetic field due to ports 1 and 2.

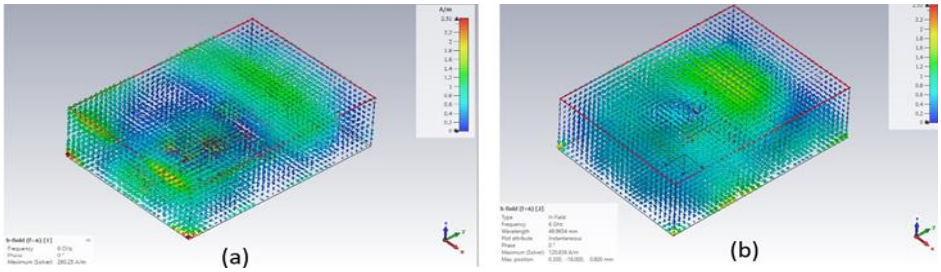

The directivity plots are displayed in Figure 16 (a) and (b) for both Excitation_port1_phi=0 and Excitation_port1_phi=90. The amount of energy that is transmitted in each direction can be shown using the directivity plot. Radiation angle is commonly shown on the x-axis and directivity on the y-axis of a polar plot. The directivity diagram for Excitation_port1_phi=0 indicates that the antenna's primary radiation is occurring in the forward (theta=0) direction. There is also backward radiation (theta = 180 degrees), but it is significantly less than the forward radiation. The Excitation_port1_phi=90 directivity plot indicates that the antenna radiates most of its power in the perpendicular direction (theta=90 degrees). It's important to note that the perpendicular radiation is significantly stronger than the radiation in the parallel direction (theta=0 degrees).

Figure 11 Excitation_port1_phi=0 and Excitation_port1_phi=90

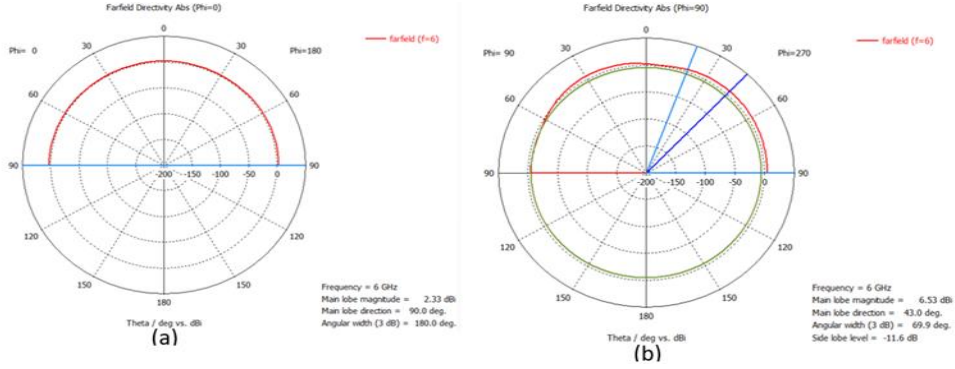

Figure 17 (a) and (b) are polar plots illustrating the antenna's far-field directivity at phi=0 and phi=90 degrees for excitation port 2's two possible excitation phases. For both excitation phases, the diagrams demonstrate that the antenna radiates a primary lobe in the forward direction (theta = 0 degrees). At 6 GHz, the magnitude of the main lobe is roughly 170 dB, and the angular extent of the main lobe is approximately 74.2 degrees.

Figure 17 Excitation_port2_phi=0 and Excitation_port2_phi=90

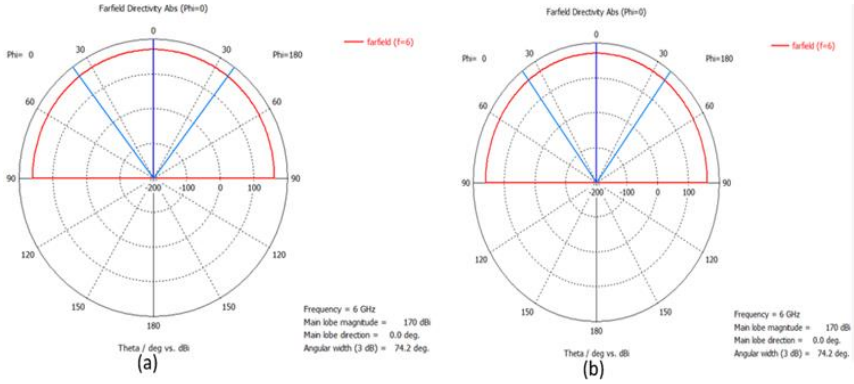

Figure 18 depicts the absolute directivity of an antenna in the far-field region, specifically at a frequency of 6 GHz. The plot illustrates that the antenna exhibits a peak directivity of 65.1 dBi when oriented in the forward direction (theta=0 degrees). As the angle theta increases, the directivity of the system diminishes and eventually reaches a minimum value of -27.4 dBi when the angle theta is equal to 180 degrees, corresponding to the reverse direction.

Figure 12 absolute far-field

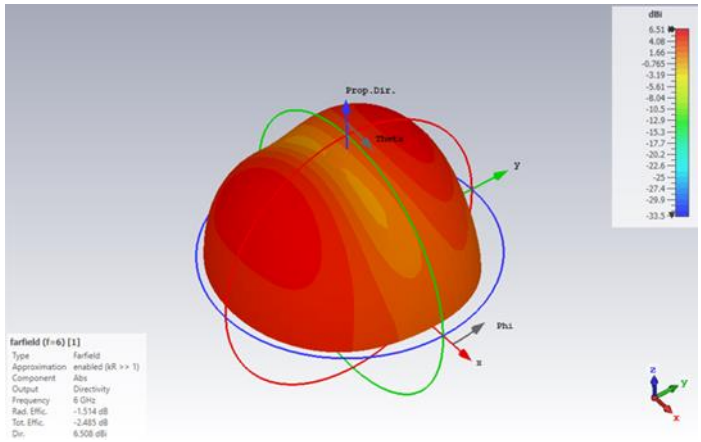

Figure 19, referred to as the Farfield_axial ratio, illustrates the relationship between the main axis and minor axis of the polarization ellipse of an antenna operating at a frequency of 6 GHz. The degree to which an antenna is polarized in a circle is indicated by its axial ratio. The polarization of the wave emitted by a circularly polarized antenna varies with time.

Figure 13 Farfield_axial ratio

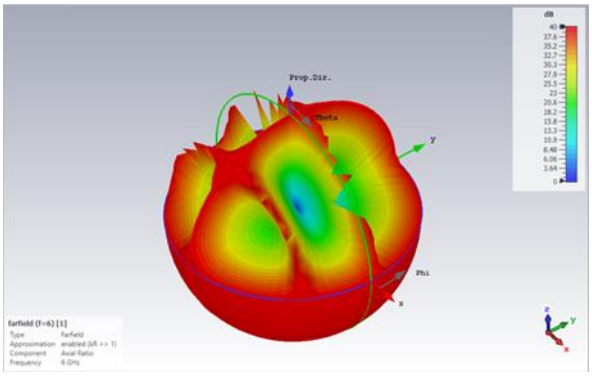

The pair of polar plots depicts the polarization phase of an antenna's far field for two distinct polarizations, namely left-handed (L) and right-handed (R). Figure 20 illustrates that the antenna exhibits linear polarization in both the left-hand (L) and right-hand (R) polarizations. The constancy of the polarization phase is observed across the entire range of angles for both polarizations.

Figure 14 far-field polarization phase

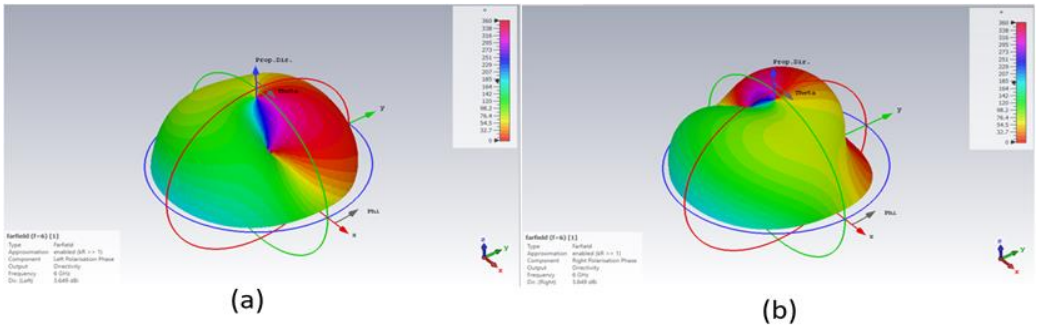

Figure 21 (a) and (b) depict the far-field radiation pattern of an antenna for left-handed (L) and right-handed (R) polarizations, respectively. The graphs indicate that the antenna has favorable directivity in the forward direction (theta=0 degrees) for both polarizations. The directivity of the left polarization exhibits a little superiority over the directivity of the right polarization.

Figure 21 far-field left and right polarization.

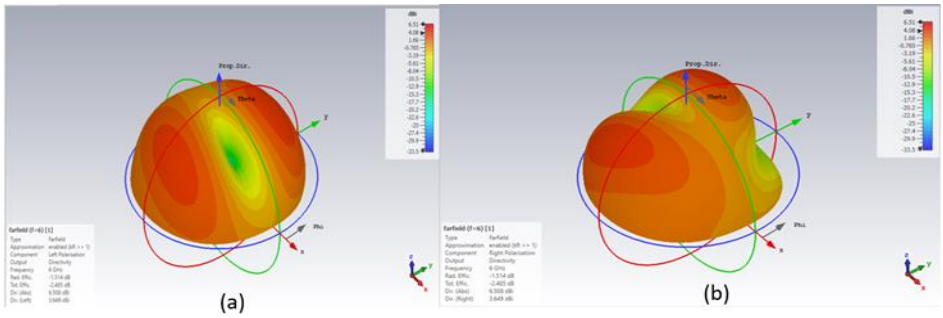

6. Conclusion

1G to 5G mobile communication networks have improved voice and data services. 5G requires high-gain antennas to support more wireless devices. 6G technology is expected to transform wireless communication by improving data throughput, latency, connectivity, dependability, and energy efficiency. Massive MIMO and IRS are two examples of MIMO technologies that are receiving significant attention in 6G research and development. Microstrip patch antennas are one of the most exciting innovations because of their small size, adaptability, and low price. The ground layer, substrate, patch, port 1, and port 2 are the basic building blocks of the initial patch antenna model. The antenna's ability to focus electromagnetic waves is improved by the ground layer's role in reflecting them toward the patch. The substrate provides support for the patch and regulates its electrical properties. The patch is responsible for the generation of electromagnetic radiation. Port 1 serves as the input port, and port 2 serves as the load port. Simulation of antenna efficacy is performed using this model. The proposed methodology entails integrating data from IoT devices with the 5G channel, optimizing data transmission efficiency, and assessing the capability of the 6G channel to handle data-intensive applications.

This research intends to contribute to the creation of effective and dependable 6G wireless communication applications. A comprehensive analysis of a patch antenna model is presented in the section on results. S-parameters for frequencies between 2.06377 GHz and 4.68255 GHz are provided in the 1-D results. These parameters reveal the network's behavior by revealing how it responds to signals of varying frequencies. Balance measurements and Y-matrix elements are presented to provide insight into system symmetry and linear electrical network behavior. A passive 6G MIMO antenna design that emphasizes high gain is presented in the 3-D results. Electric and magnetic field distributions, in addition to directivity plots, disclose how an antenna interacts with electromagnetic fields. The directivity, radiation patterns, and polarization characteristics of the antenna for various polarizations are also specified. Continued innovation in antenna design, with a focus on microstrip patch antennas, would be crucial to facilitating the capabilities of 6G networks. Future research may investigate novel materials, configurations, and integration techniques for further performance enhancement.

References

1. Savale, P. A. (2020). A comparative study of 1g to 5g generations in the wireless mobile technology: A review. Advances in Computer Science and Information Technology, 7.
2. Goyal, J., Singla, K., Akashdeep, & Singh, S. (2020). A survey of wireless communication technologies from 1G to 5G. In Second International Conference on Computer Networks and Communication Technologies: ICCNCT 2019 (pp. 613-624). Springer International Publishing.
3. Dala Pegorara Souto, V., Dester, P. S., Soares Pereira Facina, M., Gomes Silva, D., de Figueiredo, F. A. P., Rodrigues de Lima Tejerina, G., ... & Cardieri, P. (2023). Emerging MIMO technologies for 6G networks. Sensors, 23(4), 1921.
4. Sahu, A. K., Misra, N. K., Mounika, K., & Sharma, P. C. (2022). Design and Performance Analysis of MIMO Patch Antenna Using CST Microwave Studio. In Smart Systems: Innovations in Computing: Proceedings of SSIC 2021 (pp. 431-441). Springer Singapore.
5. Navarro-Ortiz, J., Romero-Diaz, P., Sendra, S., Ameigeiras, P., Ramos-Munoz, J. J., & Lopez-Soler, J. M. (2020). A survey on 5G usage scenarios and traffic models. IEEE Communications Surveys & Tutorials, 22(2), 905-929.
6. Björnson, E., Sanguinetti, L., Hoydis, J., & Debbah, M. (2015). Optimal design of energy-efficient multi-user MIMO systems: Is massive MIMO the answer?. IEEE Transactions on wireless communications,

14(6), 3059-3075.
7. Wang, Z., Zhang, J., Du, H., Wei, E. I., Ai, B., Niyato, D., & Debbah, M. (2023). Extremely large-scale MIMO: Fundamentals, challenges, solutions, and future directions. IEEE Wireless Communications.
8. Ding, Z., & Poor, H. V. (2020). A simple design of IRS-NOMA transmission. IEEE Communications Letters, 24(5), 1119-1123.
9. Cheng, Y., Li, K. H., Liu, Y., Teh, K. C., & Poor, H. V. (2021). Downlink and uplink intelligent reflecting surface aided networks: NOMA and OMA. IEEE Transactions on Wireless Communications, 20(6), 3988-4000.
10. Chen, S., Zhang, J., Zhang, J., Björnson, E., & Ai, B. (2022). A survey on user-centric cell-free massive MIMO systems. Digital Communications and Networks, 8(5), 695-719.
11. Mukherjee, A., & Kwon, H. M. (2007). Compact multi-user wideband MIMO system using multiple mode microstrip antennas. In IEEE 65th Vehicular Technology Conference - VTC2007 Spring (pp. 584–588).
12. Sanchez-Fernandez, M., Rajo-Iglesias, E., Quevedo-Teruel, O., & Pablo-Gonzalez, M. L. (2008). Spectral efficiency in MIMO systems using space and pattern diversities under compactness constraints. IEEE Transactions on Vehicular Technology, 57(3), 1637–1645.
13. Emami-Forooshani, A., & Noghanian, S. (2010). Semi-deterministic channel model for MIMO systems. Part 2: Results. IET Microwaves, Antennas & Propagation, 4(1), 26–34.
14. Chowdhury, M. H., Hossain, Q. D., Hossain, M. A., & Cheung, R. C. C. (2019). Single feed circularly polarized crescent-cut and extended corner square microstrip antennas for wireless biotelemetry. International Journal of Electrical and Computer Engineering, 9(3), 1902–1909.
15. Babu, K. V., & Anuradha, B. (2020). Design of multi-band Minkowski MIMO antenna to reduce the mutual coupling. Journal of King Saud University - Engineering Sciences, 32(1), 51–57.
16. Iqbal, A., Altaf, A., Abdullah, M., Alibakhshikenari, M., Limiti, E., & Kim, S. (2020). Modified U-shaped resonator as decoupling structure in MIMO antenna. Electronics, 9(8), 1321.
17. Sree, G. N. J., & Nelaturi, S. (2020). Semi-circular MIMO patch antenna using the neutralization line technique for UWB applications. In Microelectronics, Electromagnetics and Telecommunications (pp. 175–182). Springer, Singapore.
18. Waldschmidt, C., Kuhnert, C., Schulteis, S., & Wiesbeck, W. (2003). Compact MIMO-arrays based on polarization-diversity. In IEEE Antennas and Propagation Society International Symposium (Vol. 2, pp. 499–502).
19. Saad, W., Bennis, M., & Chen, M. (2019). A vision of 6G wireless systems: Applications, trends, technologies, and open research problems. IEEE Network, 34(3), 134–142.
20. Chanyour, T., Hmimz, Y., El Ghmary, M., & Oucamah Cherkaoui Malki, M. (2020). Delay-aware and user-adaptive offloading of computation-intensive applications with per-task delay in mobile edge computing networks. International Journal of Advanced Computer Science and Applications, 11(1).
21. Liu, Q., Sarfraz, S., & Wang, S. (2020). An overview of key technologies and challenges of 6G. In Machine Learning for Cyber Security: Third International Conference, ML4CS 2020, Guangzhou, China, October 8–10, 2020, Proceedings, Part II (Vol. 3, pp. 315–326). Springer International Publishing.
22. Zhao, Y., Zhai, W., Zhao, J., Zhang, T., Sun, S., Niyato, D., & Lam, K. Y. (2020). A comprehensive survey of 6G wireless communications. arXiv preprint arXiv:2101.03889.
23. Tariq, F., Khandaker, M. R. A., Wong, K.-K., Imran, M. A., Bennis, M., & Debbah, M. (2020). A speculative study on 6G. IEEE Wireless Communications, 27(4), 118–125.
24. Ho, T. M., Tran, T. D., Nguyen, T. T., Kazmi, S. M., Le, L. B., Hong, C. S., & Hanzo, L. (2019). Next-generation wireless solutions for the smart factory, smart vehicles, the smart grid, and smart cities. arXiv preprint arXiv:1907.10102.
25. Piran, M. J., & Suh, D. Y. (2019). Learning-driven wireless communications, towards 6G. In 2019 International Conference on Computing, Electronics & Communications Engineering (iCCECE) (pp. 219–224). IEEE.
26. Nayak, S., & Patgiri, R. (2020). 6G communication: Envisioning the key issues and challenges. arXiv preprint arXiv:2004.04024.
27. Niu, Z., Zhang, H., Chen, Q., & Zhong, T. (2019). Isolation enhancement for closely spaced E-plane patch antenna array using defect ground structure and metal-vias. IEEE Access, 7, 119375–119383.
28. Zhang, C., et al. (2022). A dual-band eight-element MIMO antenna array for future ultrathin mobile terminals. Micromachines, 13(8), 1267. https://doi.org/10.3390/mi13081267
29. Fritz-Andrade, E., Pérez-Miguel, Á., Tirado-Méndez, J. A., Vásquez-Toledo, L. A., Marcelín-Jiménez, R.,

Rodríguez-Colina, E., & Pascoe-Chalke, M. (2022). Discrete formulation of the envelope correlation coefficient for faster analysis in MIMO antenna systems. Ingeniería, investigación y tecnología, 23(4).

30. Garg, P., & Jain, P. (2020). Isolation improvement of MIMO antenna using a novel flower-shaped metamaterial absorber at 5.5GHz WiMAX band. IEEE Transactions on Circuits and Systems, 67, 675–679.
31. Tiwari, R. N., Singh, P., Kumar, P., & Kanaujia, B. K. (2022). High isolation 4-port UWB MIMO antenna with novel decoupling structure for high-speed and 5G communication. In 2022 International Conference on Electromagnetics in Advanced Applications (ICEAA) (pp. 336–339). Cape Town, South Africa.
32. Saxena, G., Chintakindi, S., Kasim, M. A., Maduri, P. K., Awasthi, Y. K., Kumar, S., ... & Dewan, C. (2022). Metasurface-inspired wideband high isolation THz MIMO antenna for nano communication, including 6G applications and liquid sensors. Nano Communication Networks, 34, 100421.
33. Khalid, M., Naqvi, S. I., Hussain, N., Rahman, M., Mirjavadi, S. S., Khan, M. J., & Amin, Y. (2020). 4-port MIMO antenna with defected ground structure for 5G millimeter-wave applications. Electronics, 9, 71.
34. Omrani, A. (2023). An ultra-wideband microstrip MIMO antenna with EBG loading for WLAN and Sub-6G applications. arXiv preprint arXiv:2303.00530.
35. Musaed, A. A., Al-Bawri, S. S., Islam, M. T., Al-Gburi, A. J. A., & Singh, M. J. (2022). Tunable compact metamaterial-based double-negative/near-zero index resonator for 6G terahertz wireless applications. Materials, 15(16), 5608.
36. Cui, M., Wu, Z., Chen, Y., Xu, S., Yang, F., & Dai, L. (2022). Low-power communications based on RIS and AI for 6G. In 2022 IEEE International Conference on Communications Workshops (ICC Workshops) (pp. 1–2). IEEE.
37. Alsudani, A., & Marhoon, H. M. (2022). Performance enhancement of microstrip patch antenna based on frequency selective surface substrate for 5G communication applications. Evolution (N. Y), 4, 7.
38. Shlezinger, N., Alexandropoulos, G. C., Imani, M. F., Eldar, Y. C., & Smith, D. R. (2021). Dynamic metasurface antennas for 6G extreme massive MIMO communications. IEEE Wireless Communications, 28(2), 106–113.
39. Dai, L., Wang, B., Wang, M., Yang, X., Tan, J., Bi, S., ... & Xu, S. (2020). Reconfigurable intelligent surface-based wireless communications: Antenna design, prototyping, and experimental results. IEEE Access, 8, 45913–45923.
40. Dutta, J., Deb, K., Tulshyan, R., & Arora, R. (2013). Approximate KKT points and a proximity measure for termination. Journal of Global Optimization, 56(4), 1463–1499.
41. Louzazni, M., Khouya, A., Al-Dahidi, S., Mussetta, M., & Amechnoue, K. (2019). Analytical optimization of photovoltaic output with Lagrange multiplier method. Optik, 199, 163379.